Journal of Materials Chemistry A

ROYAL SOCIETY OF CHEMISTRY

COMMUNICATION

View Article Online
View Journal | View Issue

Cite this: J. Mater. Chem. A, 2021, 9, 15963

Received 13th April 2021
Accepted 24th June 2021

DOI: 10.1039/d1ta03066c

rsc.li/materials-a

Why is the O3 to O1 phase transition hindered in $LiNiO_2$ on full delithiation?†

Naohiro Ikeda,[a] Itsuki Konuma,[a] Hongahally Basappa Rajendra,[b] Taira Aida[c] and Naoaki Yabuuchi *[abd]

Ni-enriched layered materials are utilized as positive electrode materials of high-energy Li-ion batteries. Because electrode reversibility is gradually lost for stoichiometric $LiNiO_2$ after continuous cycles, Ni ions are partially substituted by other metal ions (Co, Mn, Al *etc.*). However, the origin of deterioration in stoichiometric $LiNiO_2$ is still not fully understand yet. Moreover, the loss of capacities is observed only in the high voltage region (>4.1 V), which is obviously different from the failure mode observed in other electrode materials. Here, we report for the first time the origin of deterioration, which is revealed by an *in situ* X-ray diffraction study. For fully charged NiO_2, Ni ions migrate from original octahedral sites in NiO_2 slabs to face-sharing tetrahedral sites in Li layers, by which the O3 to O1 phase transition is suppresed. Note that Ni migration is a reversible process, and the Ni ions migrate back to the original octahedral sites on discharge. However, after continuous cycles, the reversibility of Ni migration is gradually lost, and Ni ions are partially left at the tetrahedral sites in Li layers. Electrode kinetics are also deteriorated because of the Ni occupation in Li layers, and the accumulation of Ni ions at tetrahedral sites results in the loss of reversible capacities in the high voltage region. This finding opens a new way to design high-capacity Ni-enriched electrode materials, leading to the development of high-energy Li-ion batteries.

Li-containing layered oxides are used for energy storage applications since the historic inception of $LiCoO_2$ in 1980.[1] $LiCoO_2$ is isostructural with α-$NaFeO_2$ whose structure consists of a cubic close packed (ccp) array of oxide ions, and Co and Li ions are filled at vacant octahedral sites in the ccp array of anionic species.[2] Neighboring CoO_6 or LiO_6 octahedra share three edges, forming CoO_2 and LiO_2 slabs. These CoO_2 and LiO_2 slabs are alternately stacked, forming the α-$NaFeO_2$-type layered structure. The α-$NaFeO_2$-type layered structure is also classified as an O3-type layered structure according to Delmas' notation.[3] Herein, "O" indicates that Li ions are located at octahedral Li sites in $LiCoO_2$, and "3" denotes that three CoO_2 slabs are found in the unit cell. When $LiCoO_2$ is charged in a Li cell, trivalent Co ions are oxidized to tetravalent Co ions. Simultaneously, Li ions are extracted from the host structure for charge compensation. Li_xCoO_2 shows an operating voltage of approximately 4 V *vs.* metallic Li and delivers a reversible capacity of ~180 mA h g^{-1} with cationic redox of Co ions. $LiCoO_2$, combined with a graphite negative electrode, is still widely used as a power source for mobile electronics applications.

Charging to high voltage (4.8 V) and removal of all Li ions from $LiCoO_2$ result in gliding of CoO_2 slabs, forming CoO_2 with an O1-type layered structure, in which octahedral sites of Li layers share faces with the CoO_6 octahedra. Large repulsive electrostatic interaction between Co and Li ions is anticipated for the O1 phase. The O1 phase transition is, therefore, allowed only for a fully delithiated phase, or a small number of Li ions is probably found at neighboring tetrahedral sites, which share edges with the CoO_6 octahedra. This observation was first evidenced in 1996 by Amatucci *et al.* using an *in situ* X-ray diffraction (XRD) study.[4] O1-type CoO_2 is isostructural with CdI_2 with space group $P\bar{3}m1$. The formation of O1 CoO_2 has also been reported in other publications.[5,6] In contrast to $LiCoO_2$, O1-type NiO_2 cannot be easily obtained even though $LiNiO_2$ is isostructural with $LiCoO_2$. The formation of O1 NiO_2 was reported after long time exposure at 4.45 V.[7] The partial formation of the O1 NiO_2 phase was also reported in $LiNiO_2$ after acid treatment.[8] The synthesis of stoichiometric $LiNiO_2$ is difficult, and often results in the formation of non-stoichiometric $Li_{1-x}Ni_xNiO_2$. Ni^{2+} ions are located at Li sites in $Li_{1-x}Ni_xNiO_2$, and these and extra Ni ions disturb the phase transition from the O3 to O1 phase.[8] Thermal instability of NiO_2 is another practical issue as an electrode material.[9,10]

[a]*Department of Chemistry and Life Science, Yokohama National University, 79-5 Tokiwadai, Hodogaya-ku, Yokohama, Kanagawa 240-8501, Japan*

[b]*Advanced Chemical Energy Research Center, Yokohama National University, 79-5 Tokiwadai, Hodogaya-ku, Yokohama, Kanagawa 240-8501, Japan*

[c]*Sumitomo Metal Mining Co. Ltd, Battery Research Laboratories, 17-3, Isoura-cho, Nihama, Ehime 792-0002, Japan*

[d]*Elements Strategy Initiative for Catalysts and Batteries, Kyoto University, f1-30 Goryo-Ohara, Nishikyo-ku, Kyoto 615-8245, Japan. E-mail: yabuuchi-naoaki-pw@ynu.ac.jp*

† Electronic supplementary information (ESI) available. See DOI: 10.1039/d1ta03066cf

Recently, Sun *et al.* developed the synthesis method of nearly stoichiometric $LiNiO_2$ at 650 °C in an oxygen atmosphere, and nearly stoichiometric $LiNiO_2$ delivers a reversible capacity of 240 mA h g^{-1}, which corresponds to 90% of the theoretical capacity of $LiNiO_2$, at a rate of 18 mA g^{-1}.[11] Nevertheless, the formation of O1 NiO_2 was not evidenced after the extraction of nearly all Li ions, and instead, an increase in the peak intensity at the 101 diffraction line was noted.[11] In this article, the phase transition process of nearly stoichiometric $LiNiO_2$ is carefully examined by *in situ* XRD and high-resolution *ex situ* synchrotron XRD studies. Our analysis reveals that Ni ions migrate to adjacent tetrahedral sites in Li layers on charging, which is a reversible process for the initial few cycles. Nevertheless, the reversible capacity in the high voltage region is gradually lost because Ni ions are in part left at tetrahedral sites in the Li layers after continuous cycles. This fact results in the loss of the reversible capacity only in the high voltage region (>4.1 V), but not in the low voltage region (<4.1 V). The finding, including the suppression of O1 phase formation in NiO_2, is clearly a new criterion to explain the deterioration of Li_yNiO_2, which potentially provides alternative approaches to design high capacity Ni-based electrode materials.

Nearly stoichiometric $LiNiO_2$ was synthesized by the methodology developed by Sun *et al.* $LiOH{\cdot}H_2O$ (Wako Chemical Co.) was crushed into fine powder by using a mortar and pestle. Thus obtained $LiOH{\cdot}H_2O$ powder was mixed with $Ni(OH)_2$ (Wako Chemical Co.) by using a mortar and pestle, and then a mixture of $LiOH{\cdot}H_2O$ and $Ni(OH)_2$ was pressed into a pellet. 3 mol% excess LiOH was utilized to compensate for the vaporization of LiOH on heating. The pellet was heated at 650 °C in an oxygen atmosphere for 12 h. The sample after calcination was stored in an Ar-filled glove box because $LiNiO_2$ reacts with moisture in air.[12] The XRD pattern and morphological character of $LiNiO_2$ discussed in this study are shown in ESI Fig. S1a,† and the sample delivers an initial reversible capacity of 220 mA h g^{-1} at 10 mA g^{-1} as shown in ESI Fig. S1b.† Selected galvanostatic charge/discharge curves are shown in Fig. 1a. Coulombic efficiency is also plotted in ESI Fig. S1c.† Although the reversible capacity deteriorated from 220 to 160 mA h g^{-1} after 30 continuous cycles, the reversible capacity is lost only in the high voltage region (>4.1 V). No capacity reduction is evidenced in the voltage region below 4.1 V, which is clearly displayed in the differential dQ/dE curves shown in Fig. 1b. The peak at 4.2 V is gradually lost after 30 continuous cycles while symmetric oxidation/reduction profiles are retained in other peaks below 4.1 V. Observed discharge capacities in different voltage regions are also plotted in Fig. 1c. Similar deterioration of the electrode reversibility in the high-voltage region is also reported in a recent publication.[13] The loss of reversible capacity only in the high voltage region suggests that the loss of reversible capacities originates from intrinsic phase transition behavior of the high voltage region as discussed in a later section. This observation also indicates that the below three failure mechanisms are eliminated and/or negligible; (1) the loss of electrical contact and isolation of particles in the composite electrode, associated with pulverization of $LiNiO_2$, (2) dissolution of active materials in electrolyte, (3) the damage to the crystal structure, for instance oxygen loss from the crystal lattice. These failure processes inevitably result in the loss of reversible capacity in the entire voltage region, which cannot explain the degradation process of $LiNiO_2$ as observed in Fig. 1. Note that the impedance is gradually increased upon electrochemical cycling (ESI Fig. S1d†). Similar degradation of reversible capacities and the growth of impedance were also reported with 4.3 V cut-off for Li_yNiO_2 (ref. 11) (4.5 V cut-off was used in this study). Because electrolyte decomposition would be ignored with 4.3 V cut-off, it is anticipated that electrolyte decomposition and surface film formation are also less responsible for the degradation process.

To assess the loss of electrode reversibility in Li_yNiO_2 in the high voltage region, *in situ* XRD data were collected, and the data were compared with those of Li_yCoO_2. The XRD pattern and electrochemical data of $LiCoO_2$ used in this study are shown in ESI Fig. S2.† *In situ* XRD patterns were obtained using an electrochemical cell equipped with a Be window and XRD diffractometer (Bruker, D8 Advance). The slurry was pasted on thin Al foil (5 μm) and used as a composite electrode for *in situ* measurements. The cell was charged at a rate of 5 mA g^{-1} and the XRD data were collected in an initial charge process. Fig. 2 compares the *in situ* XRD patterns of Li_yNiO_2 and Li_yCoO_2 with charge curves at a slow rate of 5 mA g^{-1}. Phase transition processes observed in Li_yCoO_2 are consistent with the literature,[5] and the original rhombohedral phase with a cubic close-

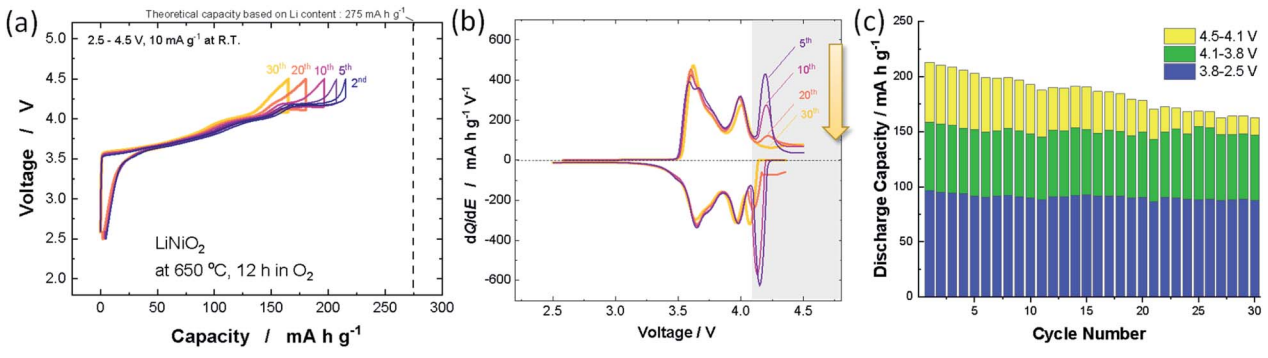

Fig. 1 (a) Galvanostatic charge/discharge curves of $LiNiO_2$ at a rate of 10 mA g^{-1}, (b) differential dQ/dE plots obtained from (a), and (c) variations in discharge capacities with different voltage ranges.

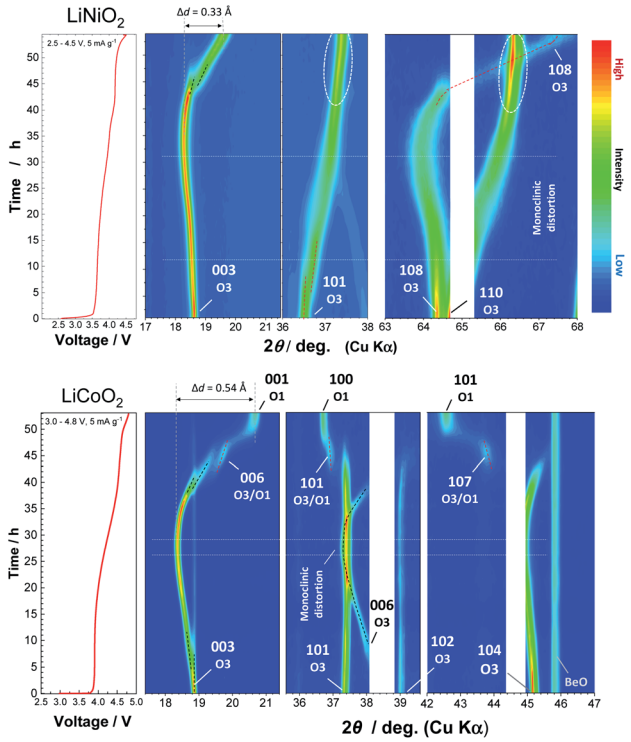

Fig. 2 Contour plots for selected ranges obtained from the *in situ* XRD patterns of $LiNiO_2$ and $LiCoO_2$ at a rate of 5 mA g^{-1}, and corresponding initial charge curves in electrochemical cells are also shown. The original *in situ* XRD data are shown in ESI Fig. S3.†

packed lattice changes into the O1 phase with a hexagonal close-packed lattice *via* the intermediate phases, monoclinic $Li_{0.5}CoO_2$ and rhombohedral $Li_{0.25}CoO_2$ with the O3/O1 intergrown layered structure (often denoted as the H1-3 phase[5]). The O3 to O1 phase transition is accompanied by a larger change in interlayer distances (a gap of 0.54 Å for $Li_{0.5}CoO_2$ and CoO_2). Gliding of CoO_2 layers is also required for the O3 to O1 phase transition. Moreover, to form the O1 phase, charging to high voltage (>4.5 V) is needed, which destabilizes the surface of oxides.[14,15] Therefore, deterioration of capacity retention is observed for $LiCoO_2$ when nearly all Li ions are extracted from the host structure (ESI Fig. 2b). In contrast, a clearly different trend is noted for $LiNiO_2$. The formation of the O1 phase is not evidenced and rhombohedral symmetry is retained after charging to 4.5 V. The 003 diffraction line for the fully charged sample is found at 19.6°, which is located at a lower diffraction angle when compared with the 001 diffraction line for O1 CoO_2 at 20.6°. In addition, a relatively small gap for interlayer distances (0.33 Å) is observed for $Li_{0.3}NiO_2$ and NiO_2 which have the longest and shortest interlayer distances, respectively. Note that the peak intensity of 101 and 110 diffraction lines is clearly increased for NiO_2 after charging to 4.5 V. The highest intensity for the 101 diffraction line is observed after charging to 4.5 V. *Ex situ* synchrotron XRD patterns of before and after charging to 4.5 V are shown in Fig. 3a. Synchrotron XRD data were collected at the beamline BL16B2 in SPring-8 synchrotron facility in Japan.[16] The measurement was conducted using an automatic powder diffraction system for Debye–Scherrer geometry using

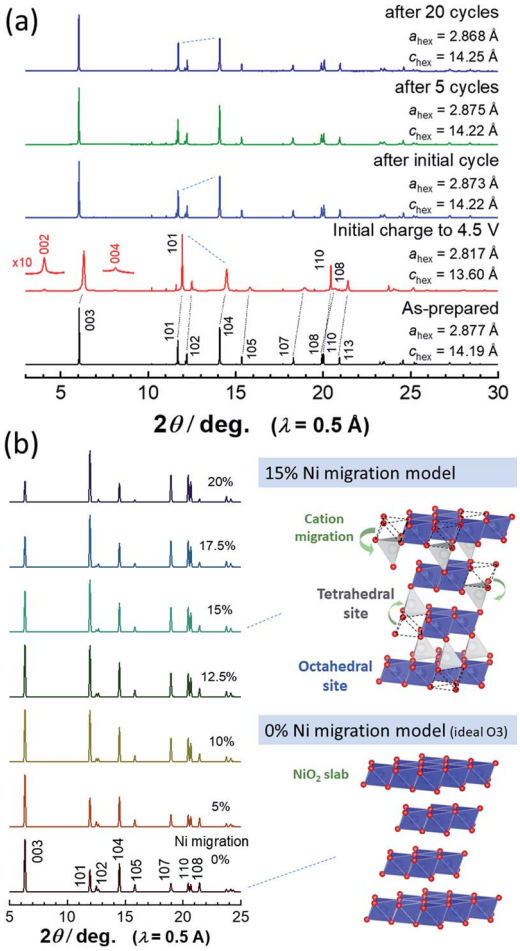

Figure 3

Fig. 3 (a) Synchrotron XRD patterns of $LiNiO_2$ before and after electrochemical cycles, and (b) simulated XRD patterns with different occupancy of Ni ions at tetrahedral 6c sites. Schematic illustrations of structural models of NiO_2 are shown, which were drawn using the program VESTA.[20]

a capillary sample. The wavelength of X-rays was calibrated to be 0.500 Å with the CeO_2 reference. A similar XRD pattern to our observation has also been reported in a publication by Sun *et al.*[11] The increase in the peak intensity of the 101 diffraction line has also been reported for $Li_xNi_{0.5}Mn_{0.5}O_2$,[17,18] and such a change originates from Ni(Li) ion occupation at tetrahedral sites (6c sites). In Na insertion layered materials, Fe migration from metal oxide slabs to face-shared tetrahedral sites in Na layers has also been reported.[19] Therefore, the XRD patterns of NiO_2 are simulated with different cation distributions (Fig. 3b). In the simulation, Ni ion migration from the original octahedral sites to face-shared tetrahedral sites in the Li layers is assumed. The intensity of the 101 and 110 lines is intensified with an increase in the enrichment of Ni ions at tetrahedral sites and less occupation at original octahedral sites. The simulated patterns in Fig. 3b clearly show that a non-negligible amount of Ni ions is occupied at tetrahedral sites in Li layers of NiO_2. When 15% of Ni ions migrate to the tetrahedral 6c sites, the intensity of the 101 diffraction line becomes higher than both

003 and 104 diffraction lines. However, peak broadening is also observed for 10*l* diffraction lines in the experimentally observed diffraction pattern of NiO_2. This observation is indicative of the presence of stacking faults, and O1 domains are partially formed in O3 NiO_2.[7] The peak broadening associated with stacking faults results in the difficulty to estimate the detailed cation distribution in NiO_2, but Ni ion migration to the tetrahedral sites is clearly non-negligible as shown in Fig. 3. To further examine possibility of the O1 phase transition for NiO_2, voltage holding is applied for 100 h at 4.5 V. However, a similar phase without voltage holding is observed as shown in ESI Fig. S4.† In addition, two new peaks at 4.07 and 8.13° appear as shown in the enlarged pattern of Fig. 3a. These two peaks are successfully assigned to 002 and 004 diffraction lines, which would originate from the presence of additional through-plane Ni ion ordering at the tetrahedral sites. The structural model of cation ordering at tetrahedral sites has not been solved yet. From these results, it is concluded that the O1 phase transition is hindered by the Ni ions at tetrahedral sites in Li layers, and thus the O3 phase is retained in NiO_2.

Note that such Ni ion migration is a reversible process. After reduction to 2.5 V in a Li cell, Ni ions migrate back to the original octahedral sites. However, changes in the peak intensity for 101 and 104 diffraction lines upon electrochemical cycling are noted in $LiNiO_2$ after 20 cycles as shown in Fig. 3a. This finding suggests that the reversibility of Ni ion migration is gradually lost upon cycling, and Ni ions are in part left at tetrahedral sites in Li layers. The results of Rietveld analysis of synchrotron XRD patterns of the as-prepared $LiNiO_2$ and the samples after the initial cycle and 20 cycles are shown in ESI Fig. S5† and 4. Rietveld refinement was carried out using RIETAN-FP software.[21] A good fitting result is obtained for as-prepared $LiNiO_2$ without the consideration of Ni ion occupation in the Li layer. After the initial cycle, a similar result is obtained without Ni ions at 6c tetrahedral sites, indicating that Ni ion migration is a reversible process. However, the intensity of the 101 diffraction line is obviously increased after 20 cycles, and an insufficient fitting result is obtained when Ni ion occupation at the tetrahedral 6c sites is not considered (Fig. 4a). The fitting result is significantly improved with the assumption of Ni ion occupation at tetrahedral sites (7%) in the Li layers as shown in Fig. 4b. In the analysis, the chemical composition is hypothesized as $Li_{0.82}NiO_2$, which is the same as that of the sample after the initial cycle because similar voltage profiles are obtained for <4.1 V region for both the initial and 20th cycles. Li ions are assumed to be kinetically trapped in the structure, leading to the gradual loss of reversible capacity in the high voltage region, associated with the enrichment of Ni ions at the tetrahedral sites. Indeed, the gradual increase in impedance upon electrochemical cycling in the fully charged state has been found as shown in ESI Fig. S1d.† The gradual loss of Ni migration reversibility is expected to originate from the kinetic limitation. Li migration is also impeded by Ni ions in the Li layer, leading to the sluggish electrode kinetics. Note that such unfavorable Ni ion migration to tetrahedral sites is effectively suppressed by substitution of Ni ions by other metal ions, leading to the improvement of electrode reversibility in the high-voltage region, which will be reported in detail elsewhere. Although stoichiometric layered materials, like $LiNiO_2$ derivatives, show excellent capacity retention as electrode materials,[22,23] now the experimentally available reversible capacity is approaching its theoretical limit. To further increase reversible capacities, Li-enrichment in the host structure is necessary.[24–27] A comparative study of degradation mechanisms for the stoichiometric and Li-enriched electrode materials leads to better understanding to design durable and high-energy positive electrode materials in the future.

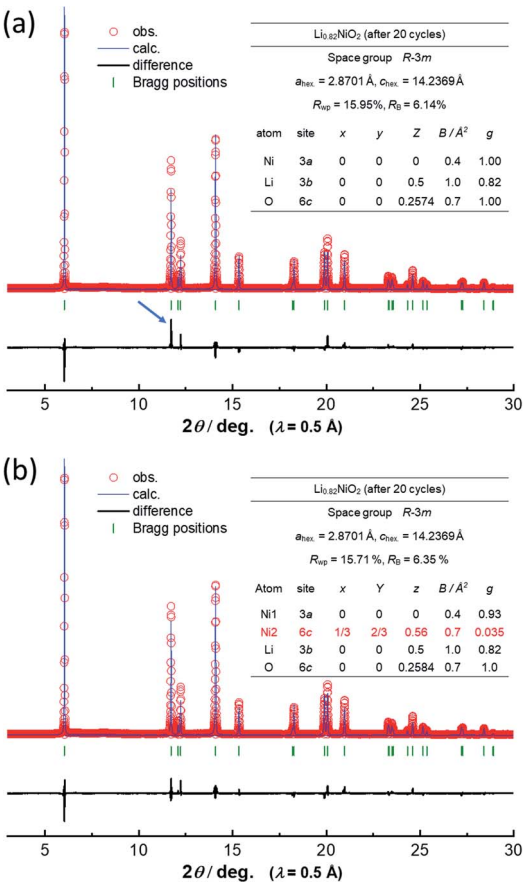

Fig. 4 Comparison of fitting results of Rietveld analysis of the synchrotron XRD pattern of Li_xNiO_2 after the 20-cycle test (a) without and (b) with the presence of Ni ions at 6c tetrahedral sites. A clear deviation between simulated and observed patterns for the 101 diffraction line is noted in (a) as marked by the blue arrow.

Author contributions

Naohiro Ikeda: investigation, formal analysis, writing – original draft. Itsuki Konuma: formal analysis. Hongahally Basappa Rajendra: investigation. Taira Aida: investigation. Naoaki Yabuuchi: conceptualization, validation, writing – review & editing, funding acquisition

Conflicts of interest

There are no conflicts to declare.

Acknowledgements

NY acknowledges the partial support from JSPS, Grant-in-Aid for Scientific Research (Grant Numbers 15H05701, 19H05816, and 21H04698), and MEXT program "Elements Strategy Initiative to Form Core Research Center (JPMXP0112101003)", and MEXT: Ministry of Education Culture, Sports, Science and Technology, Japan. The synchrotron radiation experiments were performed at the BL19B2 of SPring-8 with the approval of the Japan Synchrotron Radiation Research Institute (JASRI) (Proposal 2020A1830).

Notes and references

1 K. Mizushima, P. C. Jones, P. J. Wiseman and J. B. Goodenough, *Mater. Res. Bull.*, 1980, **15**, 783–789.
2 G. C. Mather, C. Dussarrat, J. Etourneau and A. R. West, *J. Mater. Chem.*, 2000, **10**, 2219–2230.
3 C. Delmas, C. Fouassier and P. Hagenmuller, *Physica B+C*, 1980, **99**, 81–85.
4 G. G. Amatucci, J. M. Tarascon and L. C. Klein, *J. Electrochem. Soc.*, 1996, **143**, 1114–1123.
5 Z. Chen, Z. Lu and J. R. Dahn, *J. Electrochem. Soc.*, 2002, **149**, A1604.
6 T. Motohashi, Y. Katsumata, T. Ono, R. Kanno, M. Karppinen and H. Yamauchi, *Chem. Mater.*, 2007, **19**, 5063–5066.
7 L. Croguennec, C. Pouillerie, A. N. Mansour and C. Delmas, *J. Mater. Chem.*, 2001, **11**, 131–141.
8 H. Arai, M. Tsuda, K. Saito, M. Hayashi, K. Takei and Y. Sakurai, *J. Solid State Chem.*, 2002, **163**, 340–349.
9 H. Arai, M. Tsuda, K. Saito, M. Hayashi and Y. Sakurai, *J. Electrochem. Soc.*, 2002, **149**, A401.
10 M. Guilmard, L. Croguennec, D. Denux and C. Delmas, *Chem. Mater.*, 2003, **15**, 4476–4483.
11 C. S. Yoon, D.-W. Jun, S.-T. Myung and Y.-K. Sun, *ACS Energy Lett.*, 2017, **2**, 1150–1155.
12 H. S. Liu, Z. R. Zhang, Z. L. Gong and Y. Yang, *Electrochem. Solid-State Lett.*, 2004, **7**, A190.
13 C. Lee, Y. Yokoyama, Y. Kondo, Y. Miyahara, T. Abe and K. Miyazaki, *ACS Appl. Mater. Interfaces*, 2020, **12**, 56076–56085.
14 Z. Chen and J. R. Dahn, *Electrochem. Solid-State Lett.*, 2004, **7**, A11.
15 N. Yabuuchi, Y. Kinoshita, K. Misaki, T. Matsuyama and S. Komaba, *J. Electrochem. Soc.*, 2015, **162**, A538–A544.
16 K. Osaka, Y. Yokozawa, Y. Torizuka, Y. Yamada, M. Manota, N. Harada, Y. Chou, H. Sasaki, A. Bergamaschi and M. Sato, *AIP Conf. Proc.*, 2019, **2054**, 050008.
17 H. Kobayashi, Y. Arachi, H. Kageyama and K. Tatsumi, *J. Mater. Chem.*, 2004, **14**, 40–42.
18 N. Yabuuchi, S. Kumar, H. H. Li, Y.-T. Kim and Y. Shao-Horn, *J. Electrochem. Soc.*, 2007, **154**, A566.
19 X. Li, Y. Wang, D. Wu, L. Liu, S.-H. Bo and G. Ceder, *Chem. Mater.*, 2016, **28**, 6575–6583.
20 K. Momma and F. Izumi, *J. Appl. Crystallogr.*, 2011, **44**, 1272–1276.
21 F. Izumi and K. Momma, *Solid State Phenom.*, 2007, **130**, 15–20.
22 H.-H. Ryu, G.-T. Park, C. S. Yoon and Y.-K. Sun, *J. Mater. Chem. A*, 2019, **7**, 18580–18588.
23 U.-H. Kim, G.-T. Park, P. Conlin, N. Ashburn, K. Cho, Y.-S. Yu, D. A. Shapiro, F. Maglia, S.-J. Kim, P. Lamp, C. S. Yoon and Y.-K. Sun, *Energy Environ. Sci.*, 2021, **14**, 1573–1583.
24 I. Källquist, A. J. Naylor, C. Baur, J. Chable, J. Kullgren, M. Fichtner, K. Edström, D. Brandell and M. Hahlin, *Chem. Mater.*, 2019, **31**(16), 6084–6096.
25 Y. Kobayashi, M. Sawamura, S. Kondo, M. Harada, Y. Noda, M. Nakayama, S. Kobayakawa, W. Zhao, A. Nakao, A. Yasui, H. B. Rajendra, K. Yamanaka, T. Ohta and N. Yabuuchi, *Mater. Today*, 2020, **37**, 43–55.
26 R. A. House, G. J. Rees, M. A. Pérez-Osorio, J.-J. Marie, E. Boivin, A. W. Robertson, A. Nag, M. Garcia-Fernandez, K.-J. Zhou and P. G. Bruce, *Nat. Energy*, 2020, **5**, 777–785.
27 M. Sawamura, S. Kobayakawa, J. Kikkawa, N. Sharma, D. Goonetilleke, A. Rawal, N. Shimada, K. Yamamoto, R. Yamamoto, Y. Zhou, Y. Uchimoto, K. Nakanishi, K. Mitsuhara, K. Ohara, J. Park, H. R. Byon, H. Koga, M. Okoshi, T. Ohta and N. Yabuuchi, *ACS Cent. Sci.*, 2020, **6**, 2326–2338.